


















GRB 180128A: A Second Magnetar Giant Flare Candidate from the Sculptor Galaxy

AARON C. TRIGG ¹, ERIC BURNS ¹, OLIVER J. ROBERTS ², MICHELA NEGRO ¹, DMITRY S. SVINKIN ³,
MATTHEW G. BARING ⁴, ZORAWAR WADIASINGH ^{5,6,7}, NELSON L. CHRISTENSEN ⁸, IGOR ANDREONI ^{9,6,10,*},
MICHAEL S. BRIGGS ¹¹, NICCOLÒ DI LALLA ¹², DMITRY D. FREDERIKS ³, VLADIMIR M. LIPUNOV ¹³,
NICOLA OMODEI ¹², ANNA V. RIDNAIA ³, PETER VERES ¹¹ AND ALEXANDRA L. LYSENKO ³

¹*Department of Physics & Astronomy, Louisiana State University, Baton Rouge, LA 70803, USA*

²*Science and Technology Institute, Universities Space and Research Association, 320 Sparkman Drive, Huntsville, AL 35805, USA.*

³*Ioffe Institute, 26 Politekhmicheskaya, St. Petersburg, 194021, Russia*

⁴*Department of Physics and Astronomy - MS 108, Rice University, 6100 Main Street, Houston, TX 77251-1892, USA*

⁵*Astrophysics Science Division, NASA/GSFC, Greenbelt, MD 20771, USA*

⁶*Department of Astronomy, University of Maryland, College Park, MD 20742, USA*

⁷*Center for Research and Exploration in Space Science and Technology, NASA/GSFC, Greenbelt, MD 20771, USA*

⁸*Université Côte d'Azur, Observatoire de la Côte d'Azur, CNRS, Artemis, 06304 Nice, France*

⁹*Joint Space-Science Institute, University of Maryland, College Park, MD 20742, USA*

¹⁰*Astrophysics Science Division, NASA Goddard Space Flight Center, Mail Code 661, Greenbelt, MD 20771, USA*

¹¹*Department of Space Science, University of Alabama in Huntsville, Huntsville, AL 35899, USA*

¹²*Department of Physics and Kavli Institute for Particle Astrophysics and Cosmology, Stanford University, Stanford, CA 94305, USA*

¹³*Department of Physics, Lomonosov Moscow State University, Sternberg Astronomical Institute, 119991, 13, Univeristetskij Prospekt, Moscow, Russia*

ABSTRACT

Magnetars are slowly rotating neutron stars that possess the strongest magnetic fields ($10^{14} - 10^{15}$ G) known in the cosmos. They display a range of transient high-energy electromagnetic activity. The brightest and most energetic of these events are the gamma-ray bursts (GRBs) known as magnetar giant flares (MGFs), with isotropic energy $E \approx 10^{44} - 10^{46}$ erg. There are only seven detections identified as MGFs to date: three unambiguous events occurred in our Galaxy and the Magellanic Clouds, and the other four MGF candidates are associated with nearby star-forming galaxies. As all seven identified MGFs are bright at Earth, additional weaker events remain unidentified in archival data. We conducted a search of the *Fermi* Gamma-ray Burst Monitor (GBM) database for candidate extragalactic MGFs and, when possible, collected localization data from the Interplanetary Network (IPN) satellites. Our search yielded one convincing event, GRB 180128A. IPN localizes this burst with NGC 253, commonly known as the Sculptor Galaxy. This event is the second MGF in modern astronomy to be associated with this galaxy and the first time two bursts are associated with a single galaxy outside our own. Here, we detail the archival search criteria that uncovered this event and its spectral and temporal properties, which are consistent with expectations for a MGF. We also discuss the theoretical implications and finer burst structures resolved from various binning methods. Our analysis provides observational evidence for an eighth identified MGF.

Keywords: Gamma-ray bursts(629) — Magnetars(992)

1. INTRODUCTION

A magnetar is a type of neutron star (NS) characterized by an extremely strong magnetic field, $> 10^{14}$ G (Usov 1984; Duncan & Thompson 1992; Paczynski 1992; Thompson & Duncan 1995, 1996; Kaspi et al. 2003). There are about thirty identified magnetars within our Galaxy (Olausen & Kaspi 2014) and are associated with star-forming regions (Gaensler 2004). These objects display a wide variety of high-energy transient activity: from short (sub-second) GRBs

* Neil Gehrels Fellow

to burst forests with hundreds or thousands of bursts within tens of minutes, to MGFs, the most energetic class of transient events from magnetars (see, e.g., [Kaspi & Beloborodov 2017](#), for a recent review).

MGFs are characterized by an intense initial pulse (“spike”) typically showing a millisecond-long rise time, peak energy in the gamma-ray band (\sim MeV), and total isotropic-equivalent energy $E_{\text{iso}} \gtrsim 10^{44}$ erg. In the three most proximate MGFs, observations show that a long, decaying tail with a duration of several hundred seconds follows this pulse, the intrinsic energy of which is of the order of a few 10^{44} erg. The rotation of the NS periodically modulates this tail. Given the extremely high peak luminosities of the initial spikes, detection of these emissions is possible for magnetars located in galaxies of the local group up to a distance of ~ 10 Mpc ([Burns et al. 2021](#)) by sensitive instruments such as *Fermi*-GBM. Furthermore, it has been shown in previous studies that a fraction ($\sim 2\%$) of MGFs from nearby galaxies masquerade as short GRBs ([Palmer et al. 2005](#); [Ofek 2007](#); [Hurley 2011](#); [Svinkin et al. 2015](#); [Burns et al. 2021](#)). In contrast, at extragalactic distances, the modulated tail indicative of a MGF is too faint to be observed with current instruments due to limitations in their sensitivity ([Hurley et al. 2005](#)). Given these current limitations, the best method to identify extragalactic MGF candidates is by looking for events displaying the distinct property of the prompt gamma-ray emission that are also spatially aligned with nearby star-forming galaxies.

The current sample of MGFs counts seven events, three of which happened locally (in the Milky Way and the Large Magellanic Cloud; [Mazets et al. 1979](#); [Hurley et al. 1999](#); [Mazets et al. 1999](#); [Palmer et al. 2005](#); [Frederiks et al. 2007](#)) and, due to their exceptional brightness, saturated all observing instruments at that time. The remaining four events, GRB 051103, GRB 070201, GRB 070222, and GRB 200415A, were found to have spatial alignment in 2D with nearby star-forming galaxies M81, M31, M83, and NGC 253 (also called Sculptor galaxy), respectively ([Ofek et al. 2006](#); [Frederiks et al. 2007](#); [Mazets et al. 2008](#); [Ofek et al. 2008](#); [Hurley et al. 2010](#); [Svinkin et al. 2021](#); [Roberts et al. 2021](#); [Burns et al. 2021](#)). Despite this small sample of events, [Burns et al. \(2021\)](#) recently reported a very high intrinsic volumetric rate of $R_{\text{MGF}} = 3.8_{-3.1}^{+4.0} \times 10^5 \text{ Gpc}^{-3} \text{ yr}^{-1}$, supporting the idea that a commonly occurring progenitor, such as regular core-collapse supernovae (SN), is behind the origin of magnetars and that some may produce multiple MGFs, which would help inform our understanding of the mechanisms that cause them.

Section 2 relates our method in identifying and localizing this detection. A detailed analysis of *Fermi*-GBM data for the newly found event, and a side-by-side comparison with the other MGF associated with NGC 253, GRB 200415A, and a likely NS merger GRB 150101B follows in Sections 3.1. Section 3.2 covers the *Fermi* Large Area Telescope (LAT) data analysis. Sections 3.3, 3.4, and 3.5 outline our search for detections of this event in other signals. In Section 4, we discuss the relativistic wind model for MGFs and how it relates to GRB 180128A, as well as the multi-pulse characteristics seen in the lightcurves of this new MGF candidate and three others, and the implications of finding a second burst localized to NGC 253. Finally, we conclude our findings in Section 5.

2. MGF IDENTIFICATION

The *Fermi* GBM consists of 12 uncollimated Thallium-doped Sodium Iodide (NaI) detectors and two Bismuth Germanate (BGO) detectors. The NaI and BGO detectors arranged opposite sides of *Fermi* (n0-n5 and b0 on one side and n6-nb and b1 on the other), with the NaI detectors oriented to observe the entire unocculted sky. The effective spectral ranges of the NaI and BGO detectors are ~ 8 –900 keV and ~ 0.25 –40 MeV, respectively, resulting in a combined spectral range of ~ 8 keV to 40 MeV. To date, several catalogs detailing GRB data collected by the *Fermi*-GBM ([Gruber et al. 2014](#); [Von Kienlin et al. 2014](#); [Bhat et al. 2016](#); [Von Kienlin et al. 2020](#)) have been released. The events listed in these catalogs are generally longer and have longer variability timescales than MGFs ([Gruber et al. 2014](#); [Von Kienlin et al. 2014](#); [Bhat et al. 2016](#); [Von Kienlin et al. 2020](#)). The key parameters to separate MGFs from other prompt observations are the rise time and peak interval duration, but neither are available in the GRB catalogs. More information about the GBM instrument is available in [Meegan et al. \(2009\)](#).

Extragalactic candidate MGFs can be distinguished from regular short GRBs as the former show a shorter rise time and pulse duration, higher spectral energy peak, and are associated with host galaxies at distances appropriate to produce a given peak luminosity ($L_p \sim 10^{41} - 10^{47}$) at Earth. We scour the archival *Fermi*-GBM data, as we expect more MGFs (~ 2 –3) may be present, searching for MGF-like detections characterized by sharp, ms-long rise times and a peak interval duration consistent with the known MGF sample. When data are available, we collect localization data from IPN for the flagged MGF candidates. Here, we describe the data and the methods used to discern MGF candidates from the pool of GBM triggers.

In this work, we utilize the time-tagged events (TTE) data collected in the *Fermi* GBM catalog until August of 2022. TTE data are generated for each detector with a $2\mu\text{s}$ temporal resolution, with each photon tagged by the arrival time

and one of the 128 energy channels, with separate channels for the NaI and BGO detectors. To analyze the data, we use the GBM Data Tools (Goldstein et al. 2022). We then apply a Bayesian Blocks analysis (BB, Scargle et al. 2013) to search for significant pulses in the lightcurves. Since the majority of extragalactic MGFs generally have durations of < 100 ms (Burns et al. 2021, and references therein), our first event selection criterion is to select only the events in the catalog with a T_{50} smaller than 100 ms. The T_{50} is the duration over which 50% of the burst fluence accumulates. The start of the interval is when 25% of the total fluence is detected, measured between 50 keV and 300 keV. Applying the threshold to T_{50} instead of T_{90} (i.e., the duration during which 5% to 95% of the burst fluence accumulates over the same energy range) should prevent the removal of any real, fainter MGFs. We then collect *bcat detector mask*¹ information to determine the best viewing subset of detectors for a given burst. This information indicates which NaI detectors contribute to “bcat” files, which provide basic information on a given burst, such as duration, peak flux, and fluence. We can select the appropriate BGO detector data based on which side (defined above) of *Fermi* has more NaI detectors used in the bcat files. This initial selection yields a list of 137 possible MGF candidates.

Using the default parameters, we apply the BB algorithm in *astropy*² to the detector data and select events for which the most significant BB bin is shorter than 20 ms. This value is short enough to discard any longer types of GRBs but still long enough to include the entirety of the initial prompt emission of previously identified MGFs. To ensure consideration of only events with very sharp rise times, we require that the first significant BB bin happens within 10 ms from the most significant BB bin. We define significant bins as those with a signal-to-noise ratio greater than 3.5. After this step, 20 event candidates remain. We further remove events with known redshift, as the isotropic luminosity for events at these distances would exclude a MGF origin. We also eliminate the MGF previously identified by Burns et al. (2021), leading to a considered sample of 13 MGF candidates.

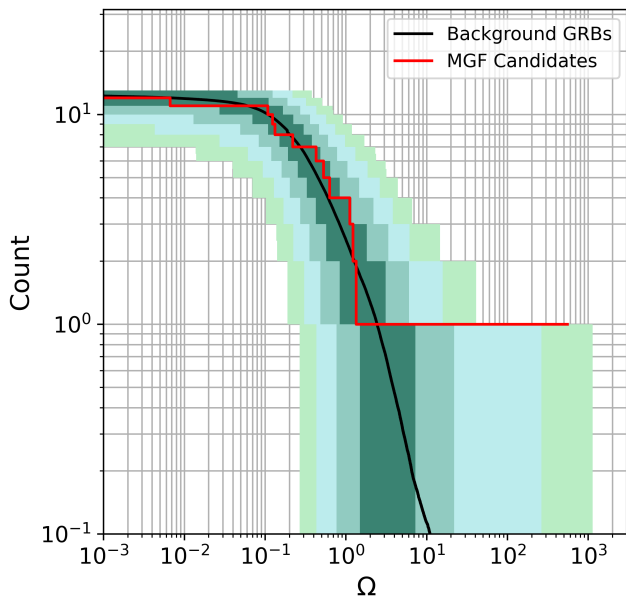


Figure 1. The significance of the selected sample of 13 MGF candidates. Ω is a ranking statistic representing the believability that a given burst is a giant flare based on 3D spatial agreement with cataloged galaxies, as described in Burns et al. (2021). The red line indicates the 13 MGF candidates while the black line represents the background distribution of GRBs. The green-shaded regions represent the 1, 2, 3, and 4 σ two-sided confidence intervals. There is a single event outlier at 3.3 σ significance; GRB 180128A.

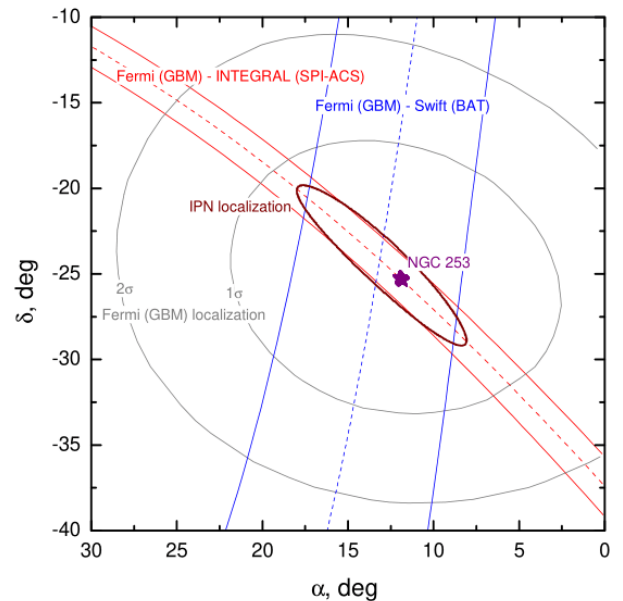


Figure 2. Final IPN localization of GRB 180128A. The localization defined by the *Fermi-INTEGRAL* (red) and *Fermi-Swift* (blue) annuli. The shown annuli widths have 3 σ confidence. The overlap of the annuli gives an ellipse (purple) with a 90% confidence area of 9.3 deg². The star marks the location of NGC 253. The initial *Fermi-GBM* localization and confidence intervals are seen in gray.

¹ <https://heasarc.gsfc.nasa.gov/w3browse/fermi/fermigbrst.html>

² https://docs.astropy.org/en/stable/api/astropy.stats.bayesian_blocks.html

The autonomous localization capability of *Fermi*-GBM is insufficient to robustly associate a GRB to a host galaxy. Thus, IPN constructs annuli for these 13 events. Two of these events were detected only by *Fermi*-GBM. Five others have detections by *Fermi*-GBM and INTEGRAL (von Kienlin et al. 2003), which only constrains the annuli that reduce the GBM localization.

The remaining six events have detections by *Fermi*-GBM, INTEGRAL, and *Swift*-BAT (Barthelmy et al. 2005). We note that none of the MGF candidates have *Swift*-BAT localizations. In quantifying the likelihood of these 13 candidates being MGFs from known galaxies, we follow the procedure in Burns et al. (2021), which compares two probability density functions (PDFs). The first one, (P^{GRB}) represents a distribution of well-localized short GRBs and compares GRB position posteriors against galaxy positions, where galaxies are weighted by distance and their integral star formation rate. Our comparison is run against a background distribution generated by rotating the positions of galaxies from the z0MG catalog (Leroy et al. 2019) and Atlas of the Local Volume Galaxies (LVG, Karachentsev et al. 2013), which then generates the confidence intervals as shown in Figure 1. The second PDF, P^{MGF} , represents the likelihood that a MGF of a given fluence at Earth could originate from a given position. The ranking statistic, $\Omega = 4\pi \sum_i P_i^{GRB} P_i^{MGF} / A_i$, the product of the probabilities of the PDFs in the i^{th} region of the sky of area A_i , represents the believability that a given burst is a giant flare based on 3D spatial agreement with the cataloged galaxies.

Among all the candidates, the GBM trigger bn180128215, hereafter GRB 180128A, was immediately identified as a strong candidate, standing out against the background distribution at 3.3σ significance. The remainder of this article focuses on the detailed analysis of this event; the population study will be the subject of future work.

Initially, the event was localized to an RA = 12.3 and dec. = -26.1 degrees (J2000) by *Fermi*-GBM, with an average error ellipse radius of 5.7 degrees (Connaughton et al. 2015), detections of GRB 180128A also exist for *Swift*-BAT (Barthelmy et al. 2005) outside of its coded field of view, and INTEGRAL SPI-ACS (von Kienlin et al. 2003). The IPN refined the localization to 9.3 deg^2 , which is centered on NGC 253, as shown in Figure 2. In further investigating this event as having a MGF origin, we perform spectral and temporal analyses for this burst.

3. PROMPT MGF ANALYSIS

For GRB 180128A, we analyze the *Fermi*-GBM data and search for signals in the *Fermi* LAT. We then compare the results with those from two other GRBs with a confident progenitor classification, allowing us to compare the characteristics of GRB 180128A with those of a known MGF and a GRB produced by another source.

3.1. *Fermi* GBM Analysis of GRB 180128A

GRB 180128A triggered GBM on January 28th, 2018 at 05:09:56.60 UT. We generate responses for detectors viewing that position within 60° of their boresight. The initial T_{50} and T_{90} durations of GRB 180128A were found to be 48 ± 51 ms and 208 ± 400 ms, respectively (Von Kienlin et al. 2020). These error bars are typical for short-duration bursts where the total fluence is almost comparable to background fluctuations in GBM. Reanalyzing this event using BB analytical techniques (Scargle et al. 2013), we find a duration (T_{BB}) of 155 ms.

We initially fit the differential energy spectrum of GRB 180128A with models typically employed for GRBs (Von Kienlin et al. 2020), and also MGFs (Roberts et al. 2021; Svinkin et al. 2021; Kaspi & Beloborodov 2017). These fits included a simple power-law (PL) model and a Band function (Band et al. 1993). In addition, our spectral fitting models focused on a Comptonized function, COMPT (Gruber et al. 2014), a form common to magnetar burst studies (e.g., Lin et al. 2011). The function is a power-law of index α modulated by an exponential cutoff at a characteristic energy E_p that is close to the spectral peak in a νF_ν representation. The values of α and E_p for GRB 180128A, and the two comparison bursts are listed in Table 1 for an array of BB time bins, defining the spectral evolution of these transients. To better illustrate the soft-to-hard-to-soft evolution that is the envelope behavior of this burst, we plot four of the BB intervals of GRB 180128A. The results in Figure 4 exhibit the spectral evolution from the onset of the burst to the two peaks to the extended emission after the peaks. For clarity, we omit the third and fifth BB intervals from Figure 4. They are, however, consistent with the trend seen in the displayed intervals. Notably, this spectral evolution is reminiscent of that clearly evident in the MGF GRB 200415A.

We perform a time-integrated fit using a COMPT model to the *Fermi*-GBM data for GRB 180128A over energies 8 keV–40 MeV, and the beginning and end of the significant emission as defined by the BB analysis, the results of which

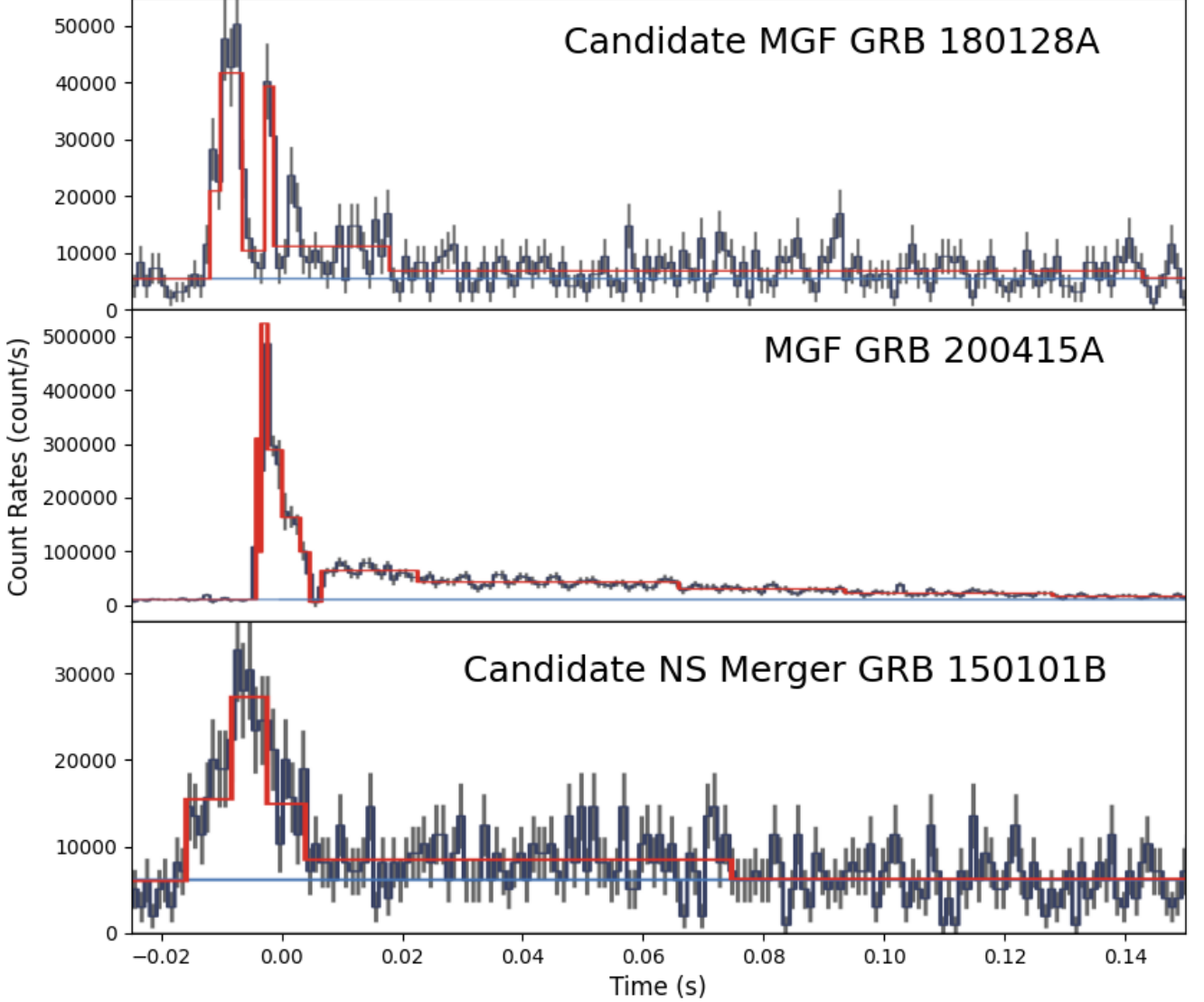


Figure 3. The lightcurves of the three events GRB 180128A, GRB 200415A, GRB 150101B, binned to a temporal resolution of 1 ms for energies from 10–500 keV. The black lines represent the raw data. The grey line shows the energy-integrated background. The red lines show the significance of the pulses above the background (grey line) using a Bayesian Blocks algorithm. At this temporal resolution GRB 180128A displays two distinct ms peaks.

are in Table 1. We note that a Band model fits the spectrum equally well but with more poorly constrained values. Using the distance to NGC 253 of 3.7 Mpc (Leroy et al. 2019, at this distance, we neglect cosmological redshift), we find an $E_{\text{iso}} = (5.9 \pm 1.0) \times 10^{44}$ erg from the fluence values of the COMPT fit to the spectrum over the BB duration of 155 s. We also find an $L_{\text{iso}} = (3.9 \pm 0.7) \times 10^{45}$ erg s $^{-1}$ from the fluence and flux values for the same model fit and duration.

We first compared the spectroscopy of our burst with that for the MGF GRB 200415A (Svinkin et al. 2021; Roberts et al. 2021), the only other MGF clearly identified by *Fermi*-GBM up to now, fitting the time bins shown in the lightcurve in Figure 3. The L_{iso} and E_{iso} determinations for GRB 180128A and GRB 200415A were consistent with those expected from a MGF and are given in Table 1 for each BB time interval, along with those for GRB 150101B. For GRB 200415A and GRB 150101B, the values from our time-integrated COMPT model analysis (also listed in Table 1) were consistent with those obtained in Roberts et al. (2021) and Burns et al. (2018), respectively. It is worth noting that the E_{iso} , E_{p} , and α values list for GRB 180128A and GRB 200415A fall within the known values of all other known MGFs (Burns et al. 2021): with α ranging from around 0.0 to 1.0 and E_{p} starting around 300 keV and extending as high as several MeV.

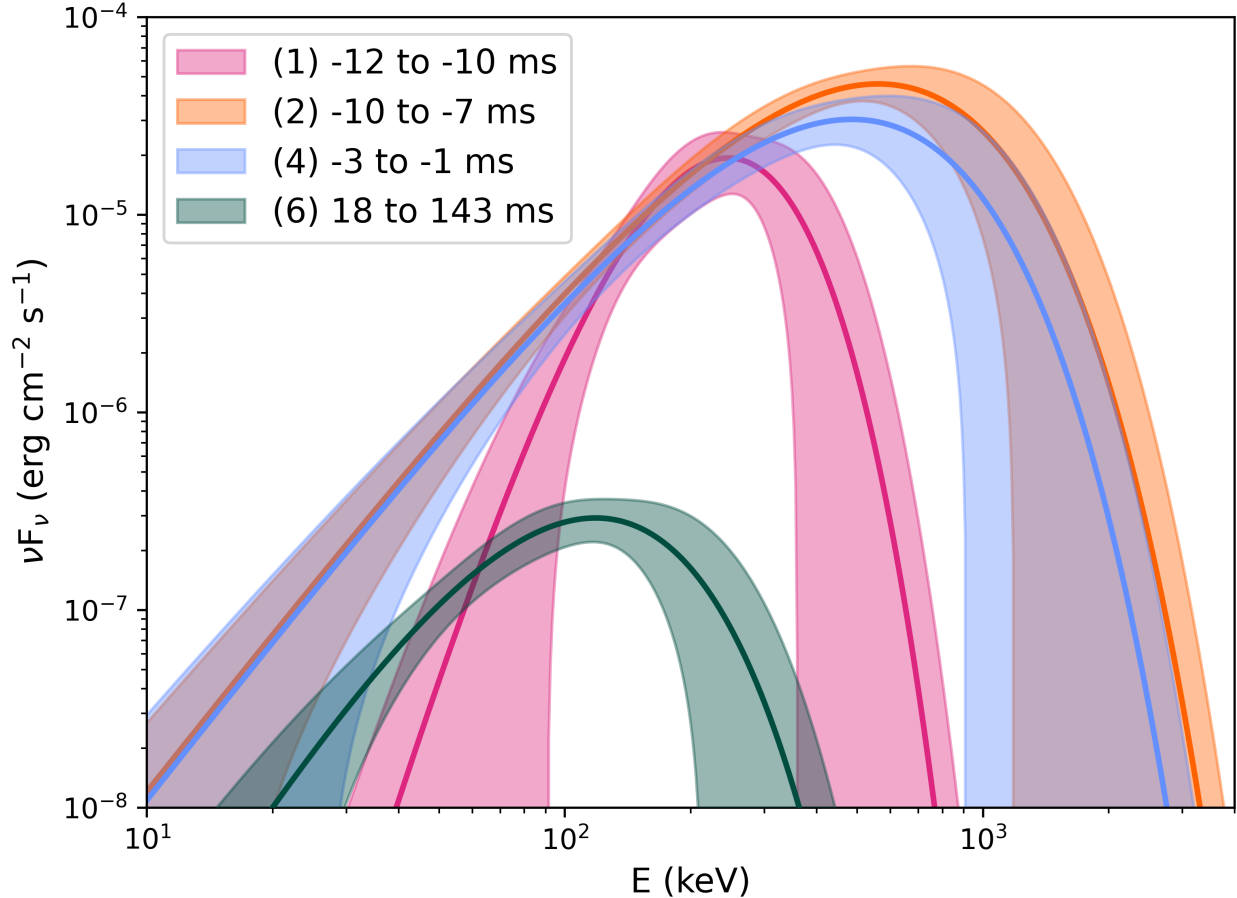


Figure 4. The spectra of GRB 180128A over four BB time intervals. The intervals show the onset of the burst (1), peak 1 (2), peak 2 (4), and the extended emission after the peaks (6). Intervals (3) and (5) are omitted for clarity yet still consistent with the trend displayed. The shaded area indicates the 1σ confidence regions

The detection of GRB 150101B by *Swift* BAT localized its position well (Cummings 2015), so that follow-up observations determined a host galaxy redshift $z = 0.134$ (Fong et al. 2016), corresponding to a source distance of 0.65 Gpc from Earth using the most recent Planck Collaboration Λ CDM cosmology parameters (Planck Collaboration et al. 2020). This distance is over two orders of magnitude greater than that of NGC 253, implying that this event is several orders of magnitude more luminous than the known Galactic MGFs. We chose GRB 150101B for comparison because it is one of the seven candidates that met all initial temporal selection criteria, but the known distance excludes a MGF origin. This transient is likely the result of a NS merger, analogous to GRB 170817A (Goldstein et al. 2017; Troja et al. 2018; Burns et al. 2018).

The lightcurve of GRB 150101B consists of a 16 ms spike followed by a longer, softer decaying tail that lasts around 64 ms, for a total event duration of around 80 ms (Burns et al. 2018), and is generated using the same criterion for determining detectors with good angles relative to the source (i.e., angle $< 60^\circ$ to boresight). Given the cosmological distance, we can not neglect cosmological redshift. Therefore, to calculate the L_{iso} and E_{iso} of the time-resolved and time-integrated spectra, we must k-correct the energy measurements (Bloom et al. 2001).

3.2. *Fermi* LAT Analysis of GRB 180128A

The *Fermi* LAT (Atwood et al. 2009) detected high-energy emission from the NGC 253 MGF in April 2020 (Ajello et al. 2021, GRB 200415A). The detection consisted of three photons between 0.48 and 1.7 GeV. The arrival time of the first photon was delayed with respect to the GBM trigger by ~ 19 s, with the last photon detected ~ 284 s later. With the tight sky localization of these photons compatible with the location of NGC 253 and the approximate

Table 1. Time-resolved spectral analysis using Bayesian Blocks

Time	E_p	α	Energy Flux (\mathcal{F})	L_{iso}	E_{iso}
(ms)	(keV)		($\times 10^{-6}$) ergs s $^{-1}$ cm $^{-2}$	$\times 10^{47}$ erg. s $^{-1}$	$\times 10^{45}$ erg
GRB 180128A					
-12:-10	250 ± 50	6.0 ± 4.9	17.1 ± 4.6	0.28 ± 0.08	0.06 ± 0.02
-10:-7 (Peak 1)	560 ± 140	0.7 ± 0.6	64.5 ± 9.5	1.1 ± 0.2	0.32 ± 0.05
-7:-3	400 ± 120	8.2 ± 13.2	10.3 ± 4.1	0.17 ± 0.07	0.07 ± 0.03
-3:-1 (Peak 2)	490 ± 150	0.7 ± 0.8	50 ± 10	0.75 ± 0.17	0.15 ± 0.03
-1:18	190 ± 20	4.9 ± 2.3	3.7 ± 0.7	0.060 ± 0.010	0.12 ± 0.02
18:143	120 ± 30	1.6 ± 1.7	0.40 ± 0.11	0.0070 ± 0.0002	0.081 ± 0.002
T_{BB} duration (155):	290 ± 50	0.6 ± 0.5	2.4 ± 0.4	0.039 ± 0.007	0.60 ± 0.10
GRB 200415A					
-4.3:-3.9 (Peak 1)	320 ± 50	0.5 ± 0.4	170 ± 20	2.7 ± 0.4	0.11 ± 0.02
-3.9:-3.4	1100 ± 700	-0.8 ± 0.3	120 ± 60	2.0 ± 0.9	0.10 ± 0.05
-3.4:-2.9 (Peak 2)	800 ± 130	-0.1 ± 0.2	490 ± 80	8.0 ± 1.3	0.40 ± 0.07
-2.9:-2.5 (Peak 3)	1100 ± 200	-0.50 ± 0.14	850 ± 140	14 ± 2	0.56 ± 0.10
-2.5:-0.5 [†]	1210 ± 120	-0.1 ± 0.1	630 ± 60	10.5 ± 1.0	2.1 ± 0.2
-0.5:3.0	2040 ± 180	-0.16 ± 0.08	600 ± 50	10.0 ± 1.0	3.4 ± 0.3
3.0:5.0*	900 ± 200	0.1 ± 0.3	110 ± 30	1.8 ± 0.4	0.36 ± 0.07
5.0:6.5*			Completely in the data gap		
6.5:22.5*	1040 ± 80	0.8 ± 0.2	124 ± 9	2.0 ± 0.2	3.3 ± 0.2
22.5:65.8	830 ± 50	0.46 ± 0.13	51 ± 3	0.84 ± 0.05	3.7 ± 0.2
65.8:93.4	590 ± 70	0.3 ± 0.2	19 ± 2	0.31 ± 0.03	0.85 ± 0.09
93.4:121.2	430 ± 50	0.8 ± 0.4	9.7 ± 1.1	0.16 ± 0.02	0.44 ± 0.05
121.2:150.3	250 ± 40	0.9 ± 0.6	3.1 ± 0.5	0.051 ± 0.007	0.15 ± 0.02
T_{BB} duration (155)^{††}:	998 ± 40	0.04 ± 0.05	56 ± 2	0.91 ± 0.04	14.2 ± 0.5
GRB 150101B					
-16:-8 (Peak 1)	1100 ± 600	-0.4 ± 0.4	16 ± 7	8000 ± 4000	6000 ± 3000
-8:-2 (Peak 1)	220 ± 70	-0.8 ± 0.3	6.3 ± 1.3	3200 ± 700	1900 ± 400
-2:4	61 ± 12	0.3 ± 1.2	1.4 ± 0.3	730 ± 150	440 ± 90
4:74	25 ± 6	-0.8 ± 1.0	0.35 ± 0.05	180 ± 30	1300 ± 200
T_{BB} duration (90):	150 ± 80	-1.5 ± 0.2	1.1 ± 0.2	550 ± 120	4100 ± 900

NOTE—The fluence is from fitting the spectrum with a Comptonized function over a combined (NaI and BGO detectors) spectral range of 8 keV to 40 MeV.

[†] Includes the saturated portion of the spectrum from about $T_0 - 2.4$ to -0.8 ms.

* Includes the data gap, from about $T_0 + 4.6$ to 6.6 ms.

^{††} This does not include the correction for the brightest part of the event that was saturated in *Fermi*-GBM as in Roberts et al. (2021), which accounts for the lower values in this study.

temporal coincidence with the MGF, this data represented the first ever *Fermi* LAT detection in the GeV energy band of emission from a magnetar.

For GRB 180128A, NGC 253 was well within the LAT field of view at the moment of the trigger and remained visible until ~ 3000 s after. We find no significant detection at the source location and place an upper limit on the source flux. We performed a likelihood analysis with `gtburst`³, using P8R3 data with TRANSIENT10e source class, and select events within a 5-degree radius from the target, with energy between 100 MeV and 10 GeV in a time window between 0 and 3000 s from the trigger time. Assuming a power law spectrum with an index $\Gamma = -2.1$, we find an energy flux upper limit of 2.3×10^{-10} erg cm $^{-2}$ s $^{-1}$. Considering an integration time of 3000 sec and the distance to NGC 253 of 3.7 Mpc, the limit on the intrinsic total energy above the LAT threshold is $E_{\text{iso}} < 1.8 \times 10^{44}$ erg at a 95% confidence

³ <https://fermi.gsfc.nasa.gov/ssc/data/analysis/scitools/gtburst.html>

level. The MGF detected by the LAT in April 2020 had an estimated intrinsic energy of $(3.6 \pm 2.1) \times 10^{45}$ erg in the 0.1–10 GeV band, almost one order of magnitude higher than the upper limit we find in this work. The non-detection of GRB 180128A clearly rules out any notion that all MGFs have a GeV counterpart of similar strength.

Yet, we cannot *a priori* exclude that there is a quasi-linear scaling of the GeV emission observed by the LAT with the soft gamma-ray luminosity detected by the GBM.

To assess this possibility and consistently compare GRB 180128A with GRB 200415A, we repeat the analysis routine with the same setup as in Ajello et al. (2021), namely with P8_TRANSIENT020E events in a time window 10–500 s from the GBM trigger. This time, we select a region of 12 degrees radius to match the analysis setup of GRB 200415A chosen to accumulate enough background statistics to allow a better fit of the Galactic diffuse and isotropic emissions. According to this setup, the upper limit at 95% C.L. on the intrinsic luminosity in the 0.1–10 GeV energy range is $L_{\text{iso}} < 2.3 \times 10^{42}$ erg/s ($E_{\text{iso}} < 1.1 \times 10^{45}$ erg), more than a factor of 11 above the predicted value given by the simple scaling of the intrinsic energetic luminosity found for GRB 200415A. The upper limits we obtain using this setup are significantly larger, by an order of magnitude, compared to the limits for GRB 180128A obtained with the previous setup and listed in Table 2. These new limits are much closer to the values listed in Table 2 for GRB 200415A.

Table 2. *Fermi*-LAT results summary

Name	Flux ($\text{cm}^{-1}\text{s}^{-1}$)	Energy Flux ($\text{erg cm}^{-1}\text{s}^{-1}$)	L_{iso} (erg s^{-1})	E_{iso} (erg)
GRB 180128A	$< 1.9 \times 10^{-6}$	$< 2.3 \times 10^{-10}$	$< 3.7 \times 10^{41}$	$< 1.8 \times 10^{44}$
GRB 200415A	$(4.1 \pm 2.2) \times 10^{-6}$	$(4.8 \pm 2.7) \times 10^{-9}$	$(7.4 \pm 4.2) \times 10^{42}$	$(3.6 \pm 2.1) \times 10^{45}$
GRB 150101B	$< 4.9 \times 10^{-6}$	$< 1.9 \times 10^{-9}$	$< 9.4 \times 10^{46}$	$< 2.8 \times 10^{50}$

NOTE—Comparison between the LAT detection of GRB 200415A and the upper limit on GRB 180128A and GRB 150101B. For the latter, we assume $z=0.134$ for the associated host galaxy ($D = 0.65$ Gpc) Fong et al. (2016), and we use the same analysis setup as for GRB 180128A (see text). All fluxes and energy fluxes measured from 0.1 to 10 GeV.

3.3. Optical

To rule out the possibility that GRB 180128A was due to other transient candidates visible in the optical band, we conduct searches of the data from the Zwicky Transient Facility (ZTF) (Graham et al. 2019; Bellm et al. 2019) and MASTER (Lipunov et al. 2010; Lipunov et al. 2022). ZTF data show no obvious candidates, ruling out a SN and the typical afterglow at the distance of NGC 253. However, there are no observations between December 12th, 2017 and July 22nd, 2018, the range which overlaps the trigger time of our event. The MASTER observations covered $\sim 3/4$ of the IPN localization up to February 4th (~ 8 days after the burst) with no optical transient detections down to ~ 17 –19 mag, which suggests that the burst was likely not associated with a SN.

3.4. Gravitational waves

The Laser Interferometer Gravitational-Wave Observatory (LIGO) (Aasi et al. 2015) and Advanced Virgo (Acernese et al. 2014) were offline at the time of the event, having ended the second observing run on August 25th, 2017⁴. Hence, there are no gravitational-wave (GW) data to determine whether this event might be due to a NS merger.

LIGO and Virgo also have searches targeting GWs produced from magnetars (Abadie et al. 2011; Abbott et al. 2021), including those associated with MGFs (Abbott et al. 2019; Macquet et al. 2021). Even in the absence of direct detection, it is possible to set upper limits on the GW energy emission. In fact, during the Galactic MGF of December 27th 2004 (Palmer et al. 2005), LIGO reported an upper limit on the energy emission (Abbott et al. 2007). However, since this initial reporting, the sensitivity of LIGO detectors has increased ~ 100 x. Given this increase in sensitivity, the

⁴ <https://www.ligo.caltech.edu/page/timeline>

LIGO-Virgo-KAGRA observations from future observing runs (Abbott et al. 2020) will provide important information for describing the energetics of identified MGFs.

3.5. Radio

Associations between fast radio bursts (FRBs) and coincident X-ray bursts from magnetars (Bochenek et al. 2020) have led to the development of models for these phenomena consistent with MGFs. Despite NGC 253 being “radio-loud” due to a prominent synchrotron radio halo (Carilli et al. 1992), to determine if there were any FRBs detected coincident with GRB 180128A, we consult the FRB⁵ (Petroff et al. 2016) and CHIME⁶ (CHIME/FRB Collaboration et al. 2021) catalogs. The FRB catalog lists two non-verified events on the same day as GRB 180128A. However, both detection localizations are far outside the IPN localization for our event. No relevant events listed in the CHIME catalog coincide with the time or location of GRB 180128A. A search of the Very Large Array archive (Perley et al. 2011) also found no observations around the time of our event.

4. DISCUSSION

Many of the characteristics seen in GRB 180128A can be explained by current MGF theory. However, it displays several properties that make it a unique event. The first being the appearance of two distinct peaks in the lightcurve. The other interesting point is that this burst was localized to the same galaxy as another known MGF, making it the first time multiple MGFs are associated with the same galaxy outside the local neighborhood. Also of interest is how different binning techniques affect how the relativistic wind structures are resolved. Here, we discuss the implications of these properties.

4.1. Physical Mechanisms and Spectral-Flux Correlations in Fermi GBM Data for the Giant Flare Candidates

The energetics analysis in Section 3 can be interpreted as a result of a large-scale crustal disruption event (Norris et al. 1991; Thompson & Duncan 1995). Due to a build-up of magnetic stresses in the crust, the stellar crust reaches a breaking point and can shear and crack, rapidly heating the local plasma. This powerful event launches a hot, relativistic pair/photon fireball with little baryonic contamination into the magnetosphere ((Thompson & Duncan 1995), accompanied by magnetic reconnection as the plasmoid is ejected. The fast initial pulse of GRB180128A is consistent with this very large release of magnetic energy (Thompson & Duncan 1995, 1996).

The classification of GRB 180128A as a MGF came from the initial selection criteria and localization. The analysis shows it is consistent with a MGF origin. Further, insights into the MGF physical emission region and mechanism originate from considerations of the spectral evolution and the coupling between spectral and flux variations. We focus on the νF_ν peak energy E_p . For the bright GRB 200415A, the values for the power law index, α , in the COMPT spectral fits are generally in the range 0 – 1 (see Table 1). This is commensurate with expectations from polar winds in MGFs due to the high opacity of Compton scattering by electrons in the strong magnetic fields (Roberts et al. 2021). For our spectral-flux correlation analysis of GRB 200415A, we employed the α values determined from the COMPT fit, which match those of Roberts et al. (2021) for Figure 5 and Figure 6a. In contrast, because the count statistics for GRB 180128A and GRB 150101B was poorer, we fixed the power-law index to $\alpha = 1.0$ and $\alpha = 0.0$, respectively, for Figure 5 and Figure 6a. These values assume both bursts have a MGF origin: GRB 180128A being lower energy, we expect an α closer to 1.0, while GRB 150101B has a much higher energy, which would lead to an expected α value closer to 0.0. Any deviation from behaviors expected from a MGF using these values would strongly disfavor a likely MGF origin. For all three bursts in Figure 6b, the adopted α values are those listed for the BB interval choice in Table 1.

Figure 5 plots the evolution of E_p values for our two selected MGF candidates plus GRB 150101B, with data for each burst acquired using 8 ms temporal binning. It displays a quasi-exponential decay for GRB 200415A on a relatively long timescale (see also Roberts et al. 2021). GRB 180128A has a more rapid decay that is quasi-exponential at its outset. In contrast, GRB 150101B exhibits E_p values with a faster decay that quickly morphs into an E_p fluctuation.

Figure 6a presents the relationship between L_{iso} and E_p , also temporally binned to 8 ms intervals. For GRBs 180128A and 200415A, we see a well-defined $L_{\text{iso}} \propto E_p^2$ relationship which is a strong indicator of relativistic Doppler boosting (Roberts et al. 2021, see also just below). The $L_{\text{iso}} \propto E_p^2$ relation is not as readily recovered for

⁵ <https://www.frbcatalog.org/>

⁶ <https://www.chime-frb.ca/catalog>

GRB 150101B, which has fewer data points. Interestingly, when plotting the $L_{\text{iso}}-E_p$ correlation using the BB intervals (omitting any data gaps or saturated data points) as in Figure 6b, the fit index is no longer 2 (i.e., L_{iso} is not $\propto E_p^2$), and differs between the MGF candidates. The fit index for GRB 180128A is greater than 3, yet there is significant dispersion in the data points that closely matches the scatter in the time-dependent analysis of Chand et al. (2021). Moreover, we observe that the $L_{\text{iso}} \propto E_p^2$ relation can be recovered when fitting the lower L_{iso} intervals that correspond to the dips in the lightcurve of GRB 200415A. The four points above the fit line for GRB 200415A displayed in Figure 6b correspond to the first four BB intervals (and thus the peaks in the lightcurve) in Table 1. This selective sampling suggests that the BB binning choice resolves the finer structures within the burst.

The dependence of the $L_{\text{iso}}-E_p$ correlation on the temporal binning protocol is not unexpected, and it provides interesting insight into the observational sampling of a MGF wind. Roberts et al. (2021) interpreted the $L_{\text{iso}} \propto E_p^2$ coupling for GRB 200415A as being the signature of a relativistic wind emanating from the magnetar pole and collimated by the field lines (essentially a flared jet) that sweeps across an observer’s line of sight as the star rotates. During this sweep, the effective Doppler factor δ_w sampled by *Fermi* GBM rises and falls, generating a spread in E_p , with $E_p \propto \delta_w$ for the photon energy Doppler blueshift, and a range in L_{iso} . For the temporally agnostic choice of fixed, 8 ms time bins, the cumulative flux in a bin tends to sample a broader range of wind axis orientations during the stellar rotation. From the perspective of the jet axis, this essentially integrates over a large solid angle $\Delta\Omega$ of the Doppler beam. Accordingly, the accumulated signal is a flux rather than an intensity and depends quadratically on the Doppler factor, i.e., $L_{\text{iso}} \propto \delta_w^2$ due to the combination of photon Doppler blueshift and time dilation in the Lorentz boost from the wind frame to that of the observer. Thus the $L_{\text{iso}} \propto E_p^2$ relationship naturally emerges, as highlighted in the analysis of Roberts et al. (2021) and Figure 6a for GRB 200415A, and also for GRB 1801128A.

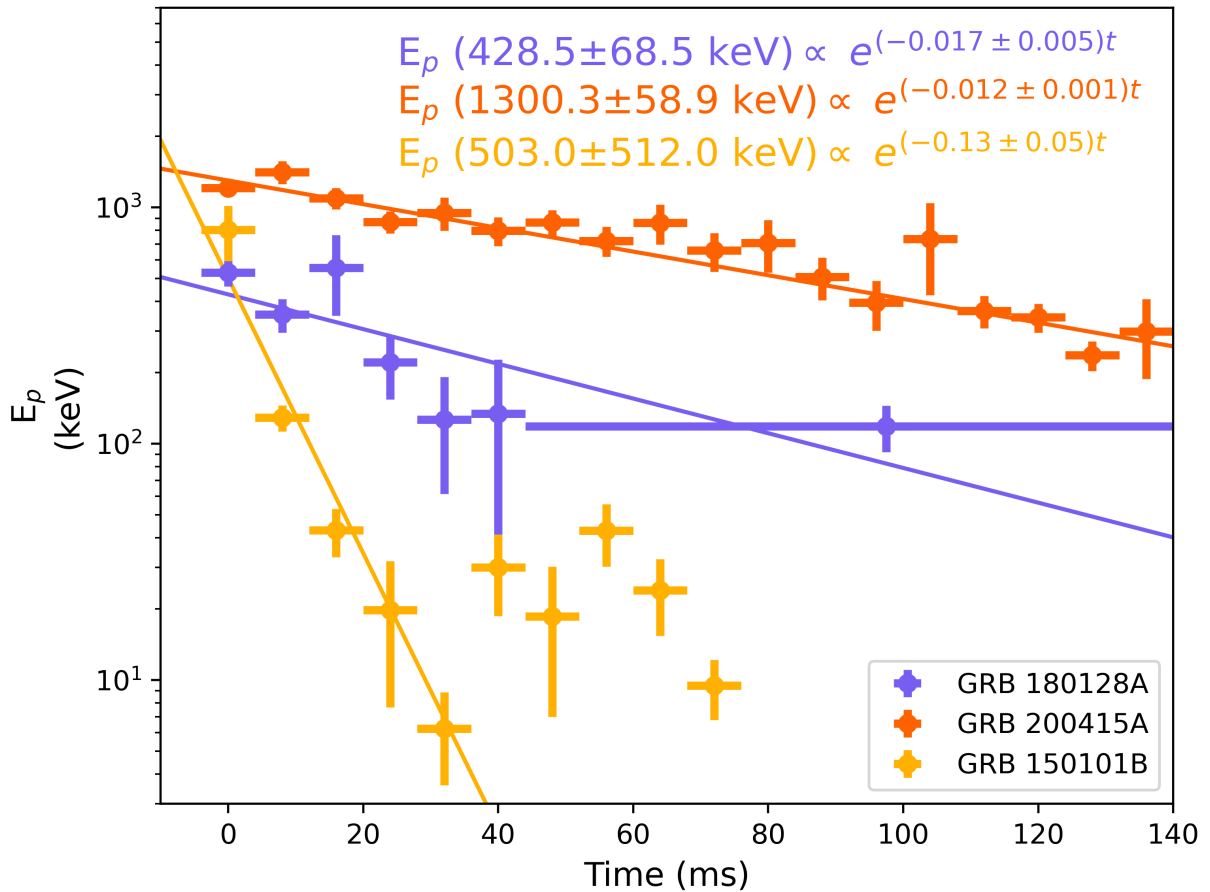


Figure 5. The Comptonized spectrum peak energy (E_p) as a function of time using a temporal binning of 8 ms. All fit errors and error bars are at the 1- σ confidence level. The zero-time reflects the GBM event start time of each GRB.

In contrast, the BB approach inherently bins on shorter timescales for higher fluxes (see Figure 3), corresponding to a narrower sampling of solid angles relative to the jet axis as the magnetar rotates. Then the detected signal scales more like intensity, i.e., flux per unit solid angle, and this has the well-known Doppler boosting dependence $L_{\text{iso}} \propto \delta_w^4$ since $\Delta\Omega \propto \delta_w^{-2}$ defines the Doppler cone. Accordingly, one would then anticipate a $L_{\text{iso}} \propto E_p^4$ in this particular extreme. It is then no surprise that the BB display in Figure 6b for GRB 200415A and GRB 180128A generates a stronger $L_{\text{iso}}-E_p$ correlation than that observed for fixed time bins in Figure 6a. The fit index being below four suggests that there is a partial sampling of the wings of the Doppler beam in the shortest BB time bins, which, in principle, possibly allows for an estimate of the ratio of the unknown rotation period to the bulk Lorentz factor $\Gamma \sim \delta_w$ of the MGF wind. Observe that the flat $L_{\text{iso}}-E_p$ correlation for GRB 150101B cannot be explained by this picture. Its poorer count statistics and anomalous light curve suggest that other conditions prevail: its wind may not be ultra-relativistic, thereby limiting its Doppler beaming, with both being consistent with GRB 150101B resulting from a NS merger as opposed to being a MGF.

To address the element of how fast the MGF winds are, we follow the time-honored GRB tradition of using the argument of transparency of the highest energy photon (of energy E_{max}) to QED pair creation $\gamma\gamma \rightarrow e^+e^-$ to bound the bulk Lorentz factor Γ of the wind. All detected photons must escape from the emission region, and relativistic Doppler beaming makes this easier as collimation of the photons increases the effective pair threshold energy (Krolik & Pier 1991; Baring 1993). The most conservative bound of $\Gamma > E_{\text{max}}/511$ keV is obtained using Doppler boosting of the 511 keV pair threshold from the wind rest frame. For the GRB 200415A MGF, Roberts et al. (2021) reported $E_{\text{max}} \sim 3$ MeV in the GBM data (about a factor of 3 higher than the typical E_p listed in Table 1) and deduced $\Gamma \gtrsim 6$, though this is well below that inferred from the *Fermi*-LAT observations of delayed GeV photons (Ajello et al. 2021, see just below). Figure 7 shows the individual counts from the TTE data of GRB 180128A for the *Fermi*-GBM BGO 1 detector, with regions (1) and (2) corresponding to the two peak intervals. Using the Bayesian method described in Roberts et al. (2021) for the on-source/off-source signal detection, a calculated probability of 0.9999896 that an excess signal above background in the 312–484 keV region of peak 1 (blue box in interval 1) can be attributed to GRB 180128A. We find no statistically significant excess source signals for the remaining energy regions. The highest energy of photons from GRB 180128A identified as being statistically significant above background is ~ 500 keV, implying a bound $\Gamma \gtrsim 1$ that is clearly much less relativistic than that for GRB 200415A. Thus, pair transparency bounds on Γ are poorly defined for GRB 180128A.

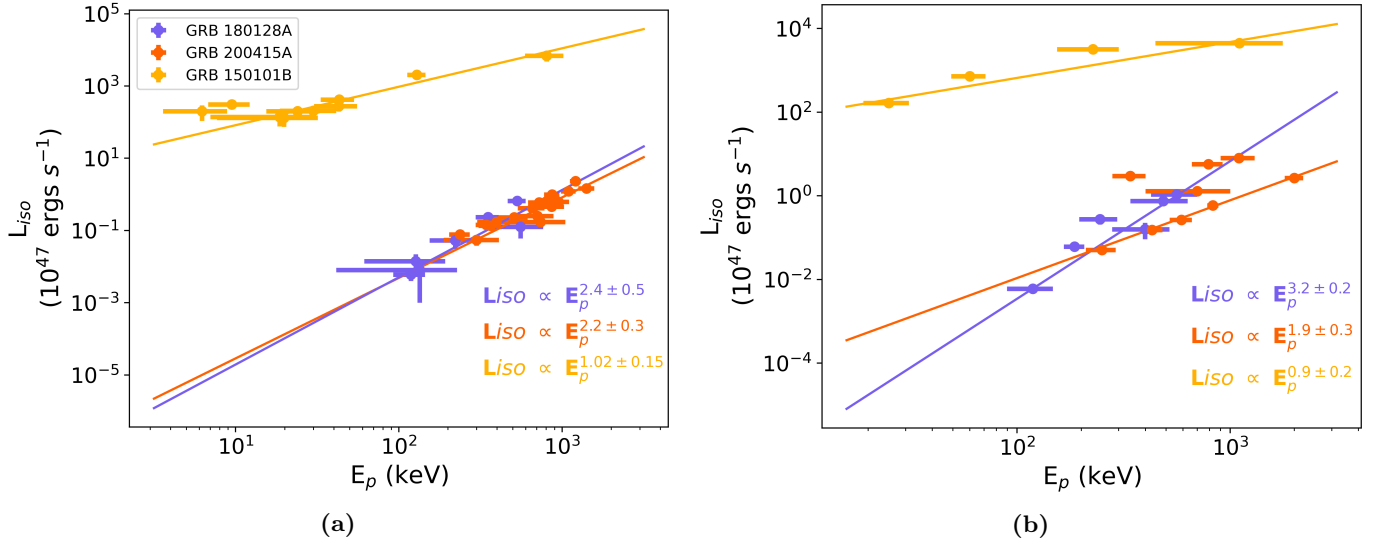


Figure 6. Flux and spectral evolution of GRB 180128A (lavender), GRB 200415A (orange), and GRB 150101B (amber), color-coded as in the inset in panel (a). **Left (a):** The correlation between L_{iso} and E_p for all three transients, revealing an approximate $L_{\text{iso}} \propto E_p^2$ relationship that is a strong signature of relativistic winds. The temporal binning for panels a is uniformly 8 ms. **Right (b):** The L_{iso} and E_p for all three transients over the BB intervals in Table 1, omitting the data gaps and saturated intervals of GRB 200415A. All fit errors and error bars are at the $1-\sigma$ confidence level.

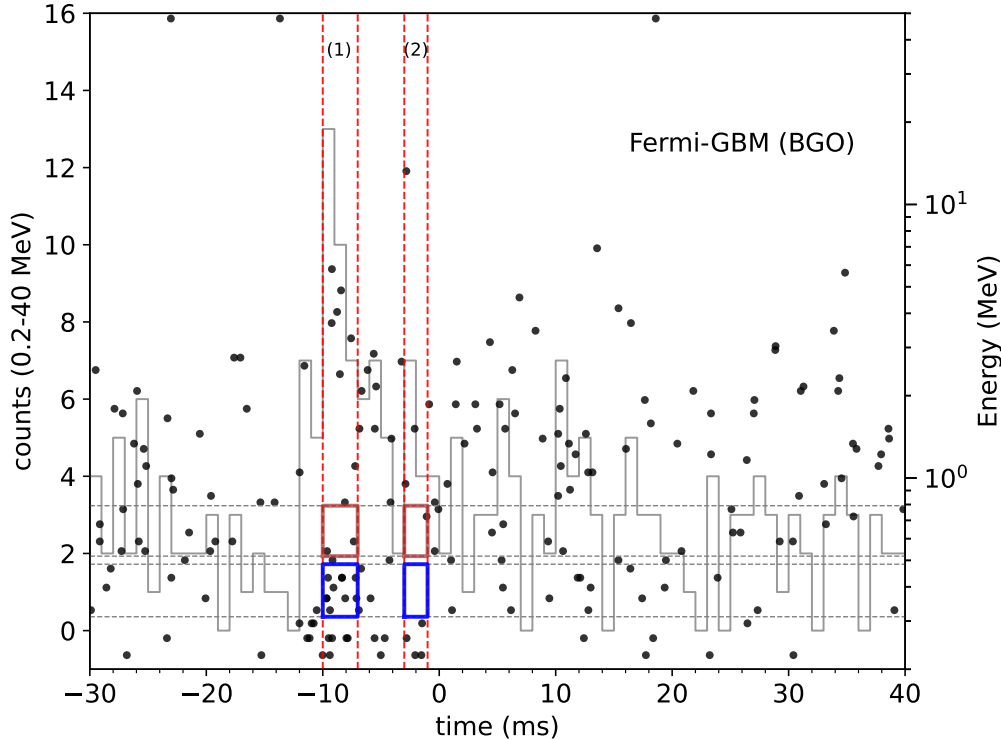


Figure 7. Individual TTE data of GBM BGO detector 1 (black dots) for GRB 180128A. The blue rectangles indicate energies from 312 to 484 keV in intervals (1) and (2), corresponding to peaks 1 and 2. The red rectangles represent energies from 518 to 792 keV for the same time intervals. We conclude that the highest photon energy associated with GRB 180128A is ~ 500 keV.

4.2. Multi-Pulse Variability

The lightcurve of GRB 180128A displays two distinct pulses at sub-ms resolution (Figure 3). This MGF candidate is the fourth event to display such behavior, the other three being GRB 070201, (Mazets et al. 2008; Ofek et al. 2008), GRB 070222 (Burns et al. 2021), and GRB 200415A (Roberts et al. 2021). In the case of GRB 070201, the temporal variability was used to argue against it having a MGF origin and raised the possibility that it was a background short GRB (Ofek et al. 2008), as such variability is consistent with short GRBs (Nakar & Piran 2002). These four account for roughly half of all likely events, the majority of which do not have sub-ms data, which may point to this being a common characteristic of MGFs.

The multi-pulse variability may imply repeated injections or varying observer geometry with the outflow. From Figure 6a, it is apparent that GRB 180128A’s interpulse traces $d \log L_{\text{iso}} / (d \log E_p) \sim 2$ as for other MGF candidates (and is distinct from GRB 150101B). This relation is compatible with the observer sampling varying Doppler factors when the outflow becomes optically thin. The multiple pulses then might be due to a similar origin from distinct persisting outflows, e.g., the observer samples a hollow conical geometry of a narrow structured jet as it sweeps past. Alternatively, these multi-pulses may be due to actual variability of energy injections from the magnetar crust and magnetosphere into the outflow. These timescales are compatible with characteristic oscillation mode periods of the magnetar, ranging from $\sim 50 - 100$ ms for the lowest-order crustal torsional modes to milliseconds for f -modes. The latter is potentially important for GW searches of MGFs (Macquet et al. 2021).

4.3. Repeating magnetar probability calculation

GRB 180128A occurred only 808 days before GRB 200415A. The median volumetric rate of $3.8 \times 10^5 \text{ Gpc}^{-3} \text{ yr}^{-1}$ (Burns et al. 2021) corresponds to 0.05 MGFs per $1.0 M_{\odot} \text{ yr}^{-1}$. Given the star formation of NGC 253 (Leroy et al. 2019) a predicted rate of $0.24 \text{ MGFs yr}^{-1}$ can be assumed. Excluding the assumption of uncorrelated events, the Poisson probability of producing these two MGFs in NGC 253 in this time frame is $\sim 9.9\%$, at 90% confidence. Rejection of

this assumption would suggest that a single, young magnetar is the source of MGFs well above the age-averaged MGF production rate for individual magnetars.

Nominally, this chance probability could be refined by accounting for the exposure and sensitivity in the observing instruments and the localization of GRB 200415A containing only a portion of NGC 253. Unfortunately, order of magnitude uncertainties currently dominate the intrinsic rate of MGFs. An unambiguous answer may be possible with more precise localizations of short GRBs. Below, we will detail the implications assuming the two events originate from a single magnetar.

Lower energy magnetar short bursts are highly correlated in time (i.e., non-Poisson). No observations exist of two MGFs from the same magnetar in our Galaxy. A time interval of 808 days is short, yet does not definitively indicate that the two MGFs emanate from the same magnetar, as $\sim 2,190$ days separated the SGR 1900 and SGR 1806 MGFs that came from different neutron stars. The magnetar crust is thought to be in a self-organized critical state (e.g., Göğüş et al. 1999; Lander 2022); short bursts have a power-law event size distribution $d \log N / d \log E_{\text{iso}} \sim -1.7$ (Cheng et al. 1996) and have temporal correlations in activity rate similar to earthquakes and associated aftershocks (Bak et al. 2002). It is unclear if the trigger for MGFs is entirely different from that for short bursts or if they are identical and MGFs are merely much rarer and larger events. A tentative calculation in Burns et al. (2021) suggests the short burst and MGF cumulative energy power-laws are compatible and could smoothly connect over 10 orders of magnitude (within large uncertainties), favoring the scenario where the short burst and MGF physical triggering mechanism are fundamentally the same. This explanation could favor a more mature magnetar where the crust has had time to solidify and form strong stresses a few decades after formation (Lander 2022) from presumably a SN.

If it is, in fact, the same magnetar, it would inform our understanding of the mechanism of MGFs and how stresses build and relax in the magnetar crust. Generally, magnetars in our Galaxy that have produced MGFs relax to less active states in the months or years following the event. The giant flares are energetic enough to putatively melt large zones of the outer crust, relieving stresses and large magnetic field twists. A second MGF would suggest a deep inner crust origin of the subsequent MGF trigger, matching expectations from some models (e.g., Lander et al. 2015; Kojima 2022). Statistics afforded by larger MGF populations are required to make definitive conclusions. Future proof of this would greatly benefit from the improved determination of the intrinsic rate uncertainties, as would newer high-energy wide-field monitors with arcminute scale localizations.

5. CONCLUSIONS

Using the distinct MGF characteristic of prompt millisecond emission, paired with IPN localization to nearby star-forming galaxies, we have developed a robust and reproducible method for searching archival data for extragalactic MGFs weaker than those previously identified. From our initial results, GRB 180128A stood out as a strong candidate MGF, supporting expectations that weak MGFs remain unidentified in archival data. Continued searches of archival *Fermi*-GBM data and the data of other missions may reveal yet more hidden MGFs. GRB 180128A was subsequently localized to NGC 253, making it the fifth likely MGF candidate localized to a nearby galaxy and the second such event localized to this specific galaxy. This localization marks the first time multiple MGFs have been found in a galaxy outside our own, supporting future studies to understand whether individual magnetars produce multiple MGFs. We have shown that the multi-pulse variability displayed in the lightcurves of GRB 180128A, and other MGFs is a common trait. Our analysis of *Fermi*-LAT data for GRB 180128A did not detect the presence of GeV photons, contrary to the case of the MGF GRB 200415A, directly showing that not all MGFs produce GeV photons.

Through our analysis and comparison of GRB 180128A and GRB 200415A, we have advanced our understanding of the physical mechanisms of these events. We extended the relativistic wind model put forth in Roberts et al. (2021) for GRB 200415A, and by using selective binning techniques, resolve the finer structures within GRB 180128A by changing the observational sampling of a MGF wind. Continued population studies will help to determine whether this model can reveal variation within the source class and whether such relativistic wind scenarios for MGFs are universal.

ACKNOWLEDGMENTS

AT, EB, MN, and OJR acknowledge NASA support under award 80NSSC21K2038. MN and ZW acknowledge the support by NASA under award number 80GSFC21M0002. MGB thanks NASA for generous support under awards 80NSSC22K0777 and 80NSSC22K1576. OJR gratefully acknowledges NASA funding through contract 80MSFC17M0022. The *Fermi*-LAT Collaboration acknowledges generous ongoing support from several agencies and institutes that have supported both the development and operation of the LAT and scientific data analysis. These include the National Aeronautics and Space Administration and the Department of Energy in the United States, the Commissariat à l’Energie Atomique and the Centre National de la Recherche Scientifique / Institut National de Physique Nucléaire et de Physique des Particules in France, the Agenzia Spaziale Italiana and the Istituto Nazionale di Fisica Nucleare in Italy, the Ministry of Education, Culture, Sports, Science and Technology (MEXT), High Energy Accelerator Research Organization (KEK), and Japan Aerospace Exploration Agency (JAXA) in Japan, the K. A. Wallenberg Foundation, the Swedish Research Council, and the Swedish National Space Board in Sweden. MASTER equipment was supported by Lomonosov MSU development program.

REFERENCES

- Aasi, J., et al. 2015, *Class. Quant. Grav.*, 32, 074001, doi: [10.1088/0264-9381/32/7/074001](https://doi.org/10.1088/0264-9381/32/7/074001)
- Abadie, J., et al. 2011, *Astrophys. J. Lett.*, 734, L35, doi: [10.1088/2041-8205/734/2/L35](https://doi.org/10.1088/2041-8205/734/2/L35)
- Abbott, B., Abbott, R., Adhikari, R., et al. 2007, *Physical Review D*, 76, 062003
- Abbott, B., et al. 2020, *Living Rev.Rel.*, 23, 3, doi: [10.1007/s41114-020-00026-9](https://doi.org/10.1007/s41114-020-00026-9)
- Abbott, B. P., et al. 2019, *Astrophys. J.*, 874, 163, doi: [10.3847/1538-4357/ab0e15](https://doi.org/10.3847/1538-4357/ab0e15)
- Abbott, R., et al. 2021, *Phys. Rev. D*, 104, 102001, doi: [10.1103/PhysRevD.104.102001](https://doi.org/10.1103/PhysRevD.104.102001)
- Acernese, F., et al. 2014, *Classical and Quantum Gravity*, 32, 024001, doi: [10.1088/0264-9381/32/2/024001](https://doi.org/10.1088/0264-9381/32/2/024001)
- Ajello, M., Atwood, W. B., Axelsson, M., et al. 2021, *Nature Astronomy*, 5, 385, doi: [10.1038/s41550-020-01287-8](https://doi.org/10.1038/s41550-020-01287-8)
- Atwood, W. B., Abdo, A. A., Ackermann, M., et al. 2009, *The Astrophysical Journal*, 697, 1071, doi: [10.1088/0004-637x/697/2/1071](https://doi.org/10.1088/0004-637x/697/2/1071)
- Bak, P., Christensen, K., Danon, L., & Scanlon, T. 2002, *PhRvL*, 88, 178501, doi: [10.1103/PhysRevLett.88.178501](https://doi.org/10.1103/PhysRevLett.88.178501)
- Band, D., Matteson, J., Ford, L., et al. 1993, *ApJ*, 413, 281, doi: [10.1086/172995](https://doi.org/10.1086/172995)
- Baring, M. G. 1993, *ApJ*, 418, 391, doi: [10.1086/173398](https://doi.org/10.1086/173398)
- Barthelmy, S. D., Barbier, L. M., Cummings, J. R., et al. 2005, *SSRv*, 120, 143, doi: [10.1007/s11214-005-5096-3](https://doi.org/10.1007/s11214-005-5096-3)
- Bellm, E. C., Kulkarni, S. R., Graham, M. J., et al. 2019, *PASP*, 131, 018002, doi: [10.1088/1538-3873/aaecbe](https://doi.org/10.1088/1538-3873/aaecbe)
- Bhat, P. N., Meegan, C. A., Von Kienlin, A., et al. 2016, *The Astrophysical Journal Supplement Series*, 223, 28
- Bloom, J. S., Frail, D. A., & Sari, R. 2001, *The Astronomical Journal*, 121, 2879
- Bochenek, C. D., Ravi, V., Belov, K. V., et al. 2020, *Nature*, 587, 59
- Burns, E., Veres, P., Connaughton, V., et al. 2018, *ApJL*, 863, L34, doi: [10.3847/2041-8213/aad813](https://doi.org/10.3847/2041-8213/aad813)
- Burns, E., Svinkin, D., Hurley, K., et al. 2021, *The Astrophysical Journal Letters*, 907, L28
- Carilli, C. L., Holdaway, M. A., Ho, P. T. P., & de Pree, C. G. 1992, *ApJL*, 399, L59, doi: [10.1086/186606](https://doi.org/10.1086/186606)
- Chand, V., Joshi, J. C., Gupta, R., et al. 2021, *Research in Astronomy and Astrophysics*, 21, 236
- Cheng, B., Epstein, R. I., Guyer, R. A., & Young, A. C. 1996, *Nature*, 382, 518, doi: [10.1038/382518a0](https://doi.org/10.1038/382518a0)
- CHIME/FRB Collaboration, Amiri, M., Andersen, B. C., et al. 2021, *ApJS*, 257, 59, doi: [10.3847/1538-4365/ac33ab](https://doi.org/10.3847/1538-4365/ac33ab)
- Connaughton, V., Briggs, M., Goldstein, A., et al. 2015, *The Astrophysical Journal Supplement Series*, 216, 32
- Cummings, J. R. 2015, *GRB Coordinates Network*, 17267, 1
- Duncan, R. C., & Thompson, C. 1992, *The Astrophysical Journal*, 392, L9
- Fong, W., Margutti, R., Chornock, R., et al. 2016, *ApJ*, 833, 151, doi: [10.3847/1538-4357/833/2/151](https://doi.org/10.3847/1538-4357/833/2/151)
- Frederiks, D. D., Palshin, V. D., Aptekar, R. L., et al. 2007, *Astronomy Letters*, 33, 19, doi: [10.1134/S1063773707010021](https://doi.org/10.1134/S1063773707010021)
- Gaensler, B. M. 2004, *Advances in Space Research*, 33, 645, doi: [10.1016/j.asr.2003.04.023](https://doi.org/10.1016/j.asr.2003.04.023)
- Goldstein, A., Cleveland, W. H., & Kocevski, D. 2022, *Fermi GBM Data Tools: v1.1.1*, <https://fermi.gsfc.nasa.gov/ssc/data/analysis/gbm>
- Goldstein, A., Veres, P., Burns, E., et al. 2017, *ApJL*, 848, L14, doi: [10.3847/2041-8213/aa8f41](https://doi.org/10.3847/2041-8213/aa8f41)

- Göğüş, E., Woods, P. M., Kouveliotou, C., et al. 1999, *ApJL*, 526, L93, doi: [10.1086/312380](https://doi.org/10.1086/312380)
- Graham, M. J., Kulkarni, S. R., Bellm, E. C., et al. 2019, *PASP*, 131, 078001, doi: [10.1088/1538-3873/ab006c](https://doi.org/10.1088/1538-3873/ab006c)
- Gruber, D., Goldstein, A., von Ahlefeld, V. W., et al. 2014, *The Astrophysical Journal Supplement Series*, 211, 12
- Hurley, K. 2011, *Advances in space research*, 47, 1337
- Hurley, K., Cline, T., Mazets, E., et al. 1999, *Nature*, 397, 41
- Hurley, K., Boggs, S. E., Smith, D. M., et al. 2005, *Nature*, 434, 1098, doi: [10.1038/nature03519](https://doi.org/10.1038/nature03519)
- Hurley, K., Rowlinson, A., Bellm, E., et al. 2010, *Monthly Notices of the Royal Astronomical Society*, 403, 342
- Karachentsev, I. D., Makarov, D. I., & Kaisina, E. I. 2013, *AJ*, 145, 101, doi: [10.1088/0004-6256/145/4/101](https://doi.org/10.1088/0004-6256/145/4/101)
- Kaspi, V. M., & Beloborodov, A. M. 2017, *ARA&A*, 55, 261, doi: [10.1146/annurev-astro-081915-023329](https://doi.org/10.1146/annurev-astro-081915-023329)
- Kaspi, V. M., Gavriil, F. P., Woods, P. M., et al. 2003, *ApJL*, 588, L93, doi: [10.1086/375683](https://doi.org/10.1086/375683)
- Kojima, Y. 2022, *ApJ*, 938, 91, doi: [10.3847/1538-4357/ac9184](https://doi.org/10.3847/1538-4357/ac9184)
- Krolik, J. H., & Pier, E. A. 1991, *ApJ*, 373, 277, doi: [10.1086/170048](https://doi.org/10.1086/170048)
- Lander, S. K. 2022, arXiv e-prints, arXiv:2209.08598. <https://arxiv.org/abs/2209.08598>
- Lander, S. K., Andersson, N., Antonopoulou, D., & Watts, A. L. 2015, *MNRAS*, 449, 2047, doi: [10.1093/mnras/stv432](https://doi.org/10.1093/mnras/stv432)
- Leroy, A. K., Sandstrom, K. M., Lang, D., et al. 2019, *ApJS*, 244, 24, doi: [10.3847/1538-4365/ab3925](https://doi.org/10.3847/1538-4365/ab3925)
- Leroy, A. K., Sandstrom, K. M., Lang, D., et al. 2019, *The Astrophysical Journal Supplement Series*, 244, 24
- Lin, L., Kouveliotou, C., Göğüş, E., et al. 2011, *ApJL*, 740, L16, doi: [10.1088/2041-8205/740/1/L16](https://doi.org/10.1088/2041-8205/740/1/L16)
- Lipunov, V., Kornilov, V., Gorbvskoy, E., et al. 2010, *Advances in Astronomy*, 2010, 1
- Lipunov, V. M., Kornilov, V. G., Zhirkov, K., et al. 2022, *Universe*, 8, 271, doi: [10.3390/universe8050271](https://doi.org/10.3390/universe8050271)
- Macquet, A., Bizouard, M.-A., Burns, E., et al. 2021, *Astrophys. J.*, 918, 80, doi: [10.3847/1538-4357/ac0efd](https://doi.org/10.3847/1538-4357/ac0efd)
- Mazets, E., Golenetskii, S., Il'Inskii, V., Aptekar', R., & Guryan, Y. A. 1979, *Nature*, 282, 587
- Mazets, E., Aptekar, R., Cline, T., et al. 2008, *The Astrophysical Journal*, 680, 545
- Mazets, E. P., Cline, T. L., Aptekar', R. L., et al. 1999, *Astronomy Letters*, 25, 635, doi: [10.48550/arXiv.astro-ph/9905196](https://doi.org/10.48550/arXiv.astro-ph/9905196)
- Meegan, C., Lichti, G., Bhat, P., et al. 2009, *The Astrophysical Journal*, 702, 791
- Nakar, E., & Piran, T. 2002, *Monthly Notices of the Royal Astronomical Society*, 330, 920
- Norris, J. P., Hertz, P., Wood, K. S., & Kouveliotou, C. 1991, *ApJ*, 366, 240, doi: [10.1086/169556](https://doi.org/10.1086/169556)
- Ofek, E. O. 2007, *The Astrophysical Journal*, 659, 339
- Ofek, E. O., Kulkarni, S., Nakar, E., et al. 2006, *The Astrophysical Journal*, 652, 507
- Ofek, E. O., Muno, M., Quimby, R., et al. 2008, *ApJ*, 681, 1464, doi: [10.1086/587686](https://doi.org/10.1086/587686)
- Olausen, S. A., & Kaspi, V. M. 2014, *The Astrophysical Journal Supplement Series*, 212, 6, doi: [10.1088/0067-0049/212/1/6](https://doi.org/10.1088/0067-0049/212/1/6)
- Paczynski, B. 1992, *Acta Astron.*, 42, 145
- Palmer, D. M., Barthelmy, S., Gehrels, N., et al. 2005, *Nature*, 434, 1107
- Perley, R., Chandler, C., Butler, B., & Wrobel, J. 2011, *The Astrophysical Journal Letters*, 739, L1
- Petroff, E., Barr, E. D., Jameson, A., et al. 2016, *PASA*, 33, e045, doi: [10.1017/pasa.2016.35](https://doi.org/10.1017/pasa.2016.35)
- Planck Collaboration, Aghanim, N., Akrami, Y., et al. 2020, *A&A*, 641, A6, doi: [10.1051/0004-6361/201833910](https://doi.org/10.1051/0004-6361/201833910)
- Roberts, O. J., Veres, P., Baring, M. G., et al. 2021, *Nature*, 589, 207, doi: [10.1038/s41586-020-03077-8](https://doi.org/10.1038/s41586-020-03077-8)
- Scargle, J. D., Norris, J. P., Jackson, B., & Chiang, J. 2013, arXiv preprint arXiv:1304.2818
- Svinkin, D., Frederiks, D., Hurley, K., et al. 2021, *Nature*, 589, 211
- Svinkin, D. S., Hurley, K., Aptekar, R. L., Golenetskii, S. V., & Frederiks, D. D. 2015, *MNRAS*, 447, 1028, doi: [10.1093/mnras/stu2436](https://doi.org/10.1093/mnras/stu2436)
- Thompson, C., & Duncan, R. C. 1995, *MNRAS*, 275, 255, doi: [10.1093/mnras/275.2.255](https://doi.org/10.1093/mnras/275.2.255)
- . 1996, *ApJ*, 473, 322, doi: [10.1086/178147](https://doi.org/10.1086/178147)
- Troja, E., Ryan, G., Piro, L., et al. 2018, *Nature Communications*, 9, 4089, doi: [10.1038/s41467-018-06558-7](https://doi.org/10.1038/s41467-018-06558-7)
- Usov, V. V. 1984, *Ap&SS*, 107, 191, doi: [10.1007/BF00649624](https://doi.org/10.1007/BF00649624)
- von Kienlin, A., Arend, N., Lichti, G. G., Strong, A. W., & Connell, P. 2003, in *Society of Photo-Optical Instrumentation Engineers (SPIE) Conference Series*, Vol. 4851, X-Ray and Gamma-Ray Telescopes and Instruments for Astronomy., ed. J. E. Truemper & H. D. Tananbaum, 1336–1346, doi: [10.1117/12.461141](https://doi.org/10.1117/12.461141)
- Von Kienlin, A., Meegan, C. A., Paciasas, W. S., et al. 2014, *The Astrophysical Journal Supplement Series*, 211, 13
- Von Kienlin, A., Meegan, C., Paciasas, W., et al. 2020, *The Astrophysical Journal*, 893, 46